Applied Catalysis B: Environmental 165 (2015) 511–518

Contents lists available at ScienceDirect

Applied Catalysis B: Environmental

journal homepage: www.elsevier.com/locate/apcatb

Carbon nitride nanosheets decorated with WO_3 nanorods: Ultrasonic-assisted facile synthesis and catalytic application in the green manufacture of dialdehydes

Jing Ding[a], Qianqian Liu[a], Zhaoyan Zhang[a], Xin Liu[a], Junqi Zhao[b], Shibiao Cheng[b], Baoning Zong[b], Wei-Lin Dai[a,*]

[a] Department of Chemistry and Shanghai Key Laboratory of Molecular Catalysis and Innovative Material, Fudan University, Shanghai 200433, PR China
[b] State Key Laboratory of Catalytic Materials and Reaction Engineering, Research Institute of Petroleum Processing, China Petroleum and Chemical Corporation, Beijing 100083, PR China

ARTICLE INFO

Article history:
Received 4 August 2014
Received in revised form
18 September 2014
Accepted 11 October 2014
Available online 22 October 2014

Keywords:
$g\text{-}C_3N_4$ nanosheets
WO_3 nanorods
Ultrasonic-assist
Green process
Catalytic oxidation

ABSTRACT

Carbon nitride nanosheets decorated with WO_3 nanorods ($WO_3/g\text{-}C_3N_4$) were fabricated via ultrasonic-assisted dispersion and conventional incipient wetness impregnation method. It is found that ultrasonic promoted the formation of $g\text{-}C_3N_4$ nanosheets efficiently. The promotion effect in the structural evolution and catalytic performance for the rod-like structure of WO_3 caused by $g\text{-}C_3N_4$ nanosheets were well studied. For the first time, the novel $WO_3/g\text{-}C_3N_4$ nanocomposites were used as efficient catalysts in the green process of dialdehydes from the selective oxidation of cycloalkene oxides using H_2O_2 as a clean oxidant, owing to the high dispersion of active sites and the strong interaction between cycloalkene oxides and the —NH or $—NH_2$ groups on the surface of $g\text{-}C_3N_4$ sheets. Here, C_3N_4 nanosheets are considered as the catalyst support and co-catalyst as well. The novel nanocomposites are very stable and can be reused for five times without obvious loss of catalytic activity.

1. Introduction

"Green Chemistry" is now a central issue in both academia and industry. Selective oxidation is a core technology for converting petroleum-based materials to useful chemicals [1]. Oxidative cleavage of cycloalkene oxides plays a key role in organic synthesis and industrial process. For instance, adipaldehyde, one of the most important value-added products in chemical and pharmaceutical field, has been used as chemosterilant, crosslinking agent, leather tanning agent, etc. Simultaneously, adipaldehyde can be applied in the production of hexamethylendiamine, which are the fundamental raw materials for the synthesis of nylon-6 and nylon-66 polymers [2,3]. However, commercial production of adipaldehyde using traditional organic synthesis method has obvious drawbacks, including the expensive raw materials, toxic oxidant (potassium permanganate or sodium periodate) and harsh reaction conditions. Accordingly, the exploration of a green and environmental-benign catalytic route for the industrial production of adipaldehyde using environmental-friendly aqueous H_2O_2 as the oxidant is still full of challenge.

Polymeric graphitic carbon nitride ($g\text{-}C_3N_4$), an appealing and potential material, has recently received considerable attention. It has been widely used in photocatalysis, fuel cells and gas storage, by virtue of its various physicochemical properties, such as excellent thermal and chemical stability, nontoxity, electrical conductivity, energy storage and gas adsorption [4]. However, the catalytic activity of $g\text{-}C_3N_4$ is still limited due to its low specific surface area and lack of active sites. Hence, tremendous efforts have been made to deal with this problem, including nanocasting with hard templates to obtain the mesoporous material [5], chemical doping with foreign elements [6,7], grafting organic molecule [8], and constructing a heterojunction $g\text{-}C_3N_4/X$ composite to achieve certain surface modification [9].

Tungsten oxide (WO_3) is regarded as a promising catalyst owing to its versatile application, including esterification [10], selective catalytic reduction of nitric oxide [11] and selective oxidative cleavage of cycloalkenes [12]. Despite of many advantages, commercial WO_3 also shows unsatisfactory catalytic activity due to the low surface area to volume ratio, insufficient active sites and leaching of tungsten species in the presence of H_2O_2. Thus, more research efforts have been made to design the heterogeneous WO_3-based

* Corresponding author. Tel.: +86 5566 4678; fax: +86 5566 5572.
E-mail address: wldai@fudan.edu.cn (W.-L. Dai).

http://dx.doi.org/10.1016/j.apcatb.2014.10.037
0926-3373/

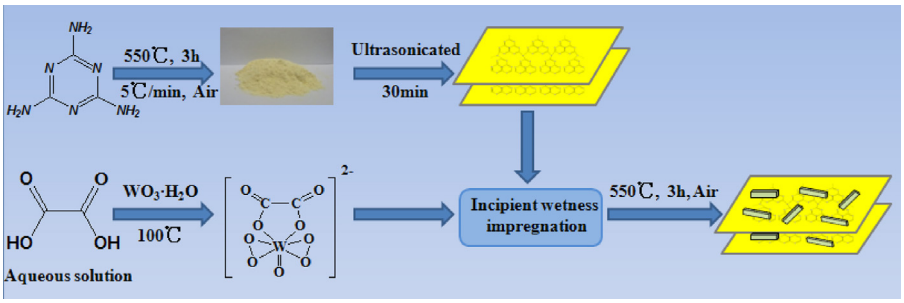

Scheme 1. Schematic representation of the synthesis process of WO_3/g-C_3N_4 catalyst.

catalyst. The good catalytic performance of several heterogeneous catalysts, including WO_3/SiO_2, W-MCM-48 and W-SBA-15 has been reported [13,14]. However, there are still some challenges in the practical application of these catalysts including the expensive raw materials, the complexity of the carrier preparation and the difficulties of large-scale production. Hence, it is urgent to seek a cheap and easy method to synthesize new kinds of WO_3-based heterogeneous catalysts.

WO_3/g-C_3N_4 nanocomposites have been attracting much attention in recent years. Katsumata et al. [15] reported the fabrication of g-C_3N_4/WO_3 by a physical mixing method and its photodegradation activity of acetaldehyde in gaseous phase. Chen et al. [16] utilized the similar synthetic method to obtain the same composite and discussed its separation mechanism of photogenerated electrons and holes in the photoexcitation. Obviously, the above composites were obtained by means of a simple mechanical method and the photoexcited electrons would transfer in the interface of the heterojunction composite between g-C_3N_4 and WO_3. However, this kind of materials cannot be recycled easily as heterogeneous catalysts in the presence of H_2O_2 due to its weak interaction between WO_3 and the support. To the best of our knowledge, there is no report involving the facile synthesis of WO_3/g-C_3N_4 with strong interaction and its catalytic application with aqueous H_2O_2 as the oxidant.

Herein, we demonstrate a green and facile ultrasonic-assisted method to prepare WO_3/g-C_3N_4 nanocomposites with excellent catalytic performance. The synthesis is quite simple, including ultrasonic dispersion, conventional incipient wetness impregnation and low-temperature calcination procedure as described in Scheme 1. The WO_3/g-C_3N_4 composite was successfully applied in the selective oxidation of cyclohexene oxide to adipaldehyde using aqueous H_2O_2 as the oxidant, exhibiting high activity and excellent recycling capacity. Simultaneously, the formation of WO_3 nanorods with the help of g-C_3N_4 nanosheets was evidenced and the possible catalytic mechanism was investigated.

2. Experimental

2.1. Preparation of WO_3/g-C_3N_4 composites

All the reagents are purchased from Sinopharm Chemical Reagent Co., Ltd. without further purification, unless otherwise specified. g-C_3N_4 nanosheets were prepared as follows. An amount of 18.0 g melamine powder was placed into a sealing alumina crucible with a cover and annealed at 550 °C under air flow for 3 h with a ramping rate of 5 °C/min. Nine grams of brown–yellow products were dispersed into 30 ml of methanol and ultrasonicated for 30 min. Subsequently, the powders were centrifuged and washed with distilled water for three times. Finally, the g-C_3N_4 nanosheets were dried at 70 °C under vacuum for overnight.

The WO_3/g-C_3N_4 composites were prepared by a conventional incipient wetness impregnation method. Typically, 0.5 g of tungstic acid was dissolved in 30 ml of oxalic acid aqueous solution (1.87 mol/l), and heated at 50 °C for 0.5 h under stirring. Then, the as-prepared g-C_3N_4 nanosheets were added to the above solution, and the temperature was risen to 100 °C for complete water evaporation. The resulting mixture was placed in an alumina crucible with a cover and calcined at 550 °C under air atmosphere for 3 h with ramping rate of 5 °C/min.

2.2. Characterizations

X-ray diffraction (XRD) patterns are recorded on a Bruker D8 advance spectrometer with Cu Kα radiation (λ = 0.154 nm), operated at 40 mA and 40 kV. The FT-IR spectra were carried out on a Nicolet Avatar-360 FT-IR spectrometer. The Laser Raman experiments were performed with a Jobin Yvon Dilor Labram I Raman spectrometer equipped with a holographic notch filter, CCD detector, and He–Ne laser radiating at 632.8 nm. Mophologies of the products were observed by using a high resolution field emission scanning electron microscope (FE-SEM). Transmission electron microscope (TEM) images were obtained on a JOEL JEM 2010 transmission electron microscope. The samples were supported on carbon-coated copper grids for the experiment. The X-ray photoelectron spectra (XPS) were obtained on a Perkin Elmer PHI 5000C ESCA system equipped with a dual X-ray source, of which the Mg Kα (1253.6 eV) anode and a hemispherical energy analyzer were used. The background pressure during data acquisition was maintained at $<10^{-6}$ Pa. Measurements were performed at a pass energy of 93.90 eV. All binding energies were calibrated using contaminant carbon (C1s = 284.6 eV).

2.3. Activity test

The liquid phase oxidation of cyclohexene oxide was performed at 35 °C with magnetic stirring at a speed of 550 r/min in a closed 25 ml regular glass reactor using 86 wt.% aqueous H_2O_2 as the oxygen donor and tributyl phosphate (TBP) as the solvent. In a typical experiment, 0.77 g of the 5 wt.% WO_3/g-C_3N_4 composite, 7.5 ml of TBP and 0.43 ml of 86 wt.% aqueous H_2O_2 were introduced into the regular glass reactor at 35 °C with magnetic stirring. The reaction was started by adding 1.00 ml of cyclohexene oxide into the above mixture and was maintained for 0.5 h. The quantitative analysis of the reaction products was carried out by gas chromatography (GC), and the determination of different products in the reaction mixture was performed by GC-mass spectroscopy (GC-MS) (see Fig. S1).

3. Results and discussion

3.1. Characterization of WO_3/g-C_3N_4 composites

As shown in Fig. 1a, the two obvious diffraction peaks at $2\theta = 27.5°$ and 13.3° match well with the (002) and (100) diffraction planes of layered g-C_3N_4 [17]. The stronger peak at 27.5°

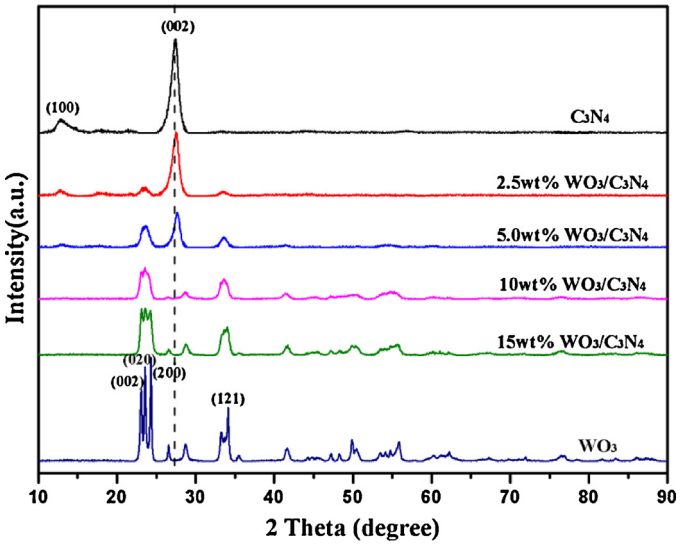

Fig. 1. XRD patterns of WO_3, g-C_3N_4 and WO_3/g-C_3N_4 composites as-prepared at 550 °C calcination temperature.

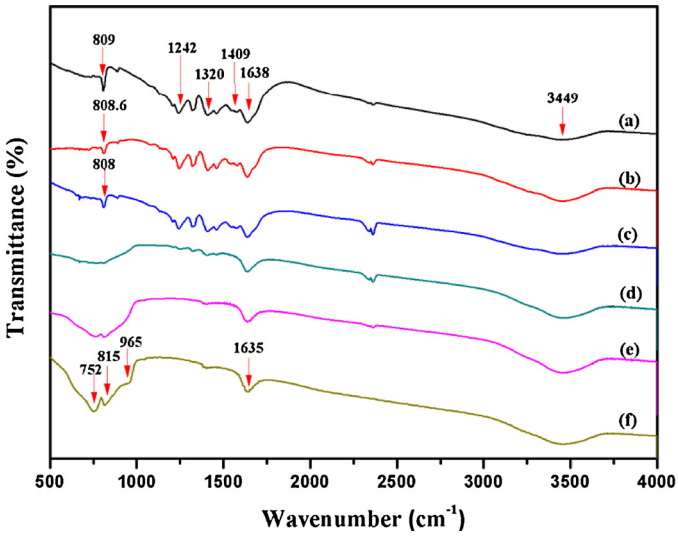

Fig. 2. FT-IR spectra of different catalysts. (a) g-C_3N_4; (b) 2.5 wt.%; (c) 5.0 wt.%; (d) 10 wt.%; (e) 15 wt.% WO_3/g-C_3N_4; and (f) WO_3.

corresponds to the interlayer stacking of the aromatic systems, whose calculated interlayer distance is 0.324 nm [18]. The weaker one at 13.3° is attributed to in-planar tris-s-triazine structural packing with the distance around 0.665 nm [19,20]. The XRD patterns of WO_3 shown in Fig. 1f accords well with the monoclinic structure (JCPDS 20-1324). For WO_3/g-C_3N_4 composites, obviously, the peaks ascribed to g-C_3N_4 grow weaker with the increasing of WO_3 content in the composites. When the amount of WO_3 reaches up to 10%, the characteristic peaks of g-C_3N_4 almost disappear, indicating that the uniform structure of g-C_3N_4-{002} facet is disturbed by WO_3 nanorods [16]. However, when the content of WO_3 is lower than 10%, the characteristic diffraction lines of WO_3 cannot be clearly found. It is presumably owing to that WO_3 crystals are highly dispersed on the surface of g-C_3N_4 nanosheets and WO_3 nanorods enter into the interlayers of the graphite-like g-C_3N_4 and interact with g-C_3N_4 nanosheets strongly. Simultaneously, the characteristic (002) peak of g-C_3N_4 shifted slightly to higher diffraction angle compared with pure g-C_3N_4, thus indicating a small expansion of the interlayers. This finding suggests that the strong interaction between WO_3 and g-C_3N_4-{002} facets and the disturbance of the packing and potential undulation of the single layers by WO_3 nanorods inserting into interlayers of g-C_3N_4 nanosheets [21].

FT-IR spectra of WO_3, g-C_3N_4 and WO_3/g-C_3N_4 composites were presented in Fig. 2. It is evident that the bands in the region ranging from 1242 to 1638 cm^{-1} (1242, 1320, 1409, 1560 and 1638 cm^{-1}) were assigned to C—NH—C and C═N stretching vibration modes of heterocycles [22,23]. Obviously, with the increasing of WO_3 content in the composites, the absorption peak at 1242 cm^{-1} assigned to C-NH-C stretching vibration weakens gradually. That is, excessive loading content of WO_3 particles may interact with —NH group of g-C_3N_4 [24]. Moreover, due to the presence of the —NH groups of heterocycles, the hydrogen bonds between —NH groups and other substrates can be easily formed. Meanwhile, the sharp band at around 809 cm^{-1} is ascribed to the breathing mode of the triazine units of g-C_3N_4 [25]. While the O–W–O stretching vibration in monoclinic-type WO_3 crystal clearly appears at 815 cm^{-1} as a broad absorption band. Obviously, the intensity of the band around 815 and 752 cm^{-1} becomes stronger with the increasing of WO_3 content in the WO_3/g-C_3N_4 composite samples [26]. When the amount of WO_3 reaches up to 10%, the characteristic absorption peaks at 807 cm^{-1} for g-C_3N_4 cannot be clearly observed, implying that the WO_3 nanorods intercalate into the interlayers of g-C_3N_4 nanosheets and interact with triazine units of g-C_3N_4 nanosheets strongly. Furthermore, with increased WO_3 amounts in the nanocomposites, the band at 809 cm^{-1} attributed to the vibrations of triazine units of g-C_3N_4 slightly red shifts, which demonstrates the existence of the strong interaction between WO_3 nanorods and triazine units of g-C_3N_4 nanosheets as well. In addition, the broad band at around 3450 cm^{-1} is associated with the primary and secondary amines and O–H stretching vibrations of surface-absorption water molecules [27,28]. Owing to the existence of the broad O–H stretching vibrations of water molecules at the same position, the sharp primary and secondary amines stretching vibrations are completely shrouded [29,30].

The morphology and microstructure of the as-obtained g-C_3N_4 and WO_3/g-C_3N_4 composites are visualized by FE-SEM, TEM and HR-TEM. As demonstrated in Fig. 3a, the as-synthesized g-C_3N_4 exhibits a sheet-like structure. The morphology of g-C_3N_4 nanosheets is similar to that previously reported. The ultrathin g-C_3N_4 nanosheets can be obtained by modified liquid exfoliating of as-prepared bulk g-C_3N_4 in methanol [31]. The thickness of the C_3N_4 nanosheets determined by atomic force microscopy (AFM) ranges from 0.3 to 0.7 nm, which further illustrates that ultrasonic-assisted synthesis of carbon nitride nanosheets leads to much lower thickness and larger BET surface area (see Fig. S2) [24]. Fig. 3b–e shows the typical FE-SEM, TEM and HR-TEM images of WO_3/g-C_3N_4 composites with 5 and 10 wt.% WO_3 contents. From Fig. 3b (FE-SEM), it can be clearly observed that small WO_3 nanorods are decorated on the g-C_3N_4 nanosheets surface. Moreover, combined with Fig. 3c, it also can be obviously seen that WO_3 nanorods are well scattered over g-C_3N_4 nanosheets, which is beneficial for the strong interaction between the reactants and the active sites. As shown in the low magnified TEM image of 5 wt.% WO_3/g-C_3N_4 in Fig. 3d, WO_3 exhibits the rectangle rod-like morphology with the crystallite size of around 11 nm, identical to the results in Table 1. It is also found that the WO_3 nanorods are well dispersed on the surface of g-C_3N_4 nanosheets and only few nanorods agglomerate, being consistent well with the results from XRD patterns. The formation of WO_3 nanorods is mainly attributed to the presence of the lamellar structure of g-C_3N_4 nanosheets, which prompt the radial growth of WO_3 particles formed in the process of conventional incipient wetness impregnation. Interestingly, the formation of WO_3 nanorods between the interlayers of g-C_3N_4 nanosheets enlarged the BET surface area of g-C_3N_4 (see Table 1). With small

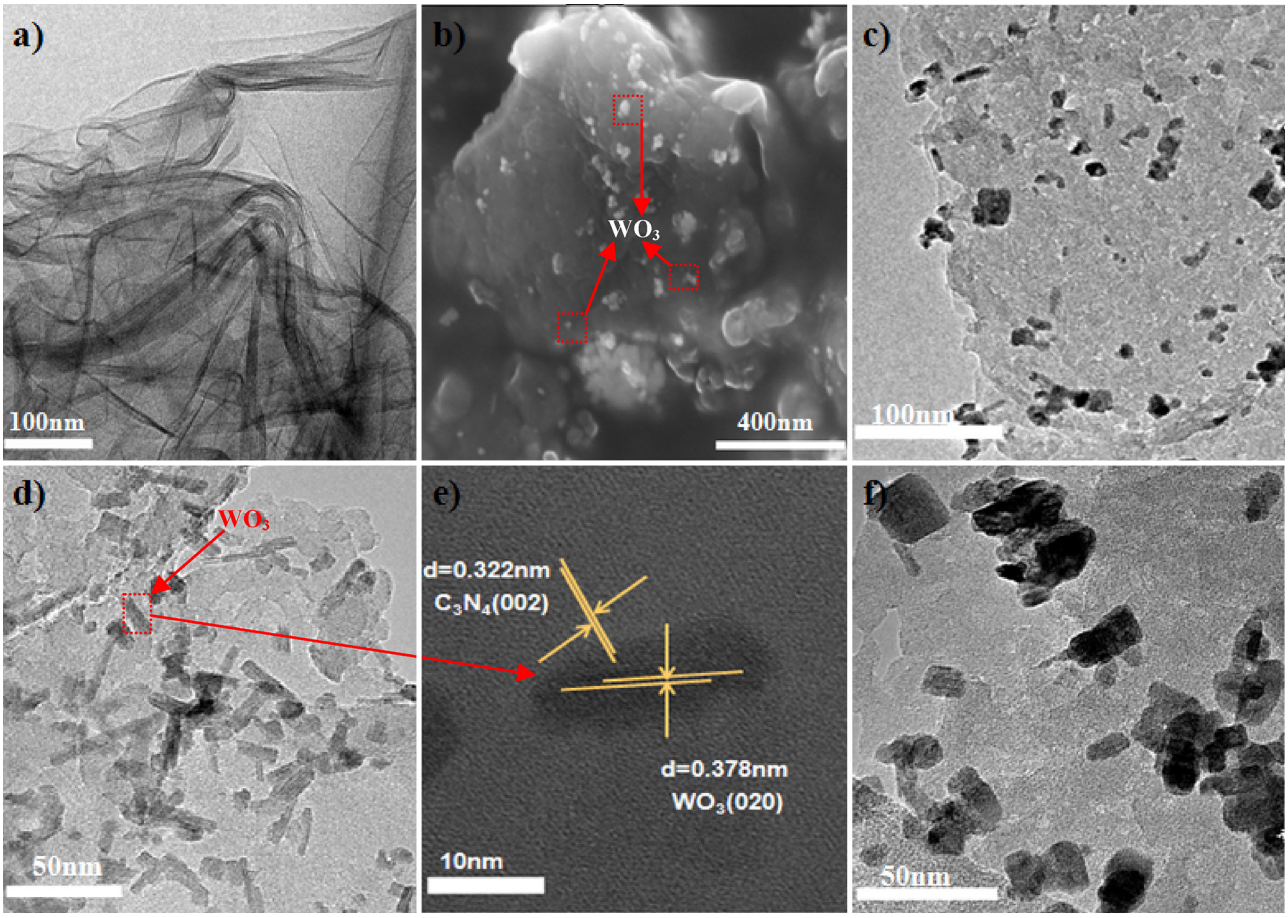

Fig. 3. TEM images of (a) g-C_3N_4 nanosheets; (c, d) 5.0 wt.% WO_3/g-C_3N_4 composites; (f) 10 wt.% WO_3/g-C_3N_4 composites; HR-TEM of images of (e) 5.0 wt.% WO_3/g-C_3N_4; FE-SEM images of (b) 5.0 wt.% WO_3/g-C_3N_4 composites.

Table 1
The physicochemical parameters of the composite.

Entry	Samples	BET specific surface area ($m^2\ g^{-1}$)	Crystallite size (nm)
1	g-C_3N_4	15	–
2	2.5% WO_3/g-C_3N_4	62	9
3	5.0% WO_3/g-C_3N_4	62	11
4	10% WO_3/g-C_3N_4	41	18
5	15% WO_3/g-C_3N_4	19	22
6	WO_3	12	44

amount of WO_3 species decorated into the nanostructure of g-C_3N_4, the BET surface area increased by four times as that of the pristine g-C_3N_4 (15–62 m^2/g), suggesting that g-C_3N_4 nanosheets were unfolded by WO_3 nanorods to increase the BET surface area, and tungsten oxide species can be well dispersed on the surface of g-C_3N_4 nanosheets to get more active reaction sites. As compared to the pristine g-C_3N_4 and WO_3 or the mechanical mixture, the formation of WO_3 nanorods between the interlayers of g-C_3N_4 nanosheets enlarged greatly the BET surface area of the composite from g-C_3N_4 and WO_3. Fig. 3e is the representative HR-TEM image of 5 wt.% WO_3/g-C_3N_4. The different orientation and lattice spacing of WO_3 nanorods and g-C_3N_4 nanosheets can be clearly observed. Particularly, one lattice spacing of 0.378 nm can be indexed to the (020) direction of monoclinic WO_3 (d = 0.377 nm). The other with d = 0.322 nm matches well with the crystal facet (002) of g-C_3N_4. Therefore, an integration interface between WO_3-{020} and g-C_3N_4-{002} is formed, which also further illustrates that there is strong interaction between WO_3 nanorods and g-C_3N_4 nanosheets.

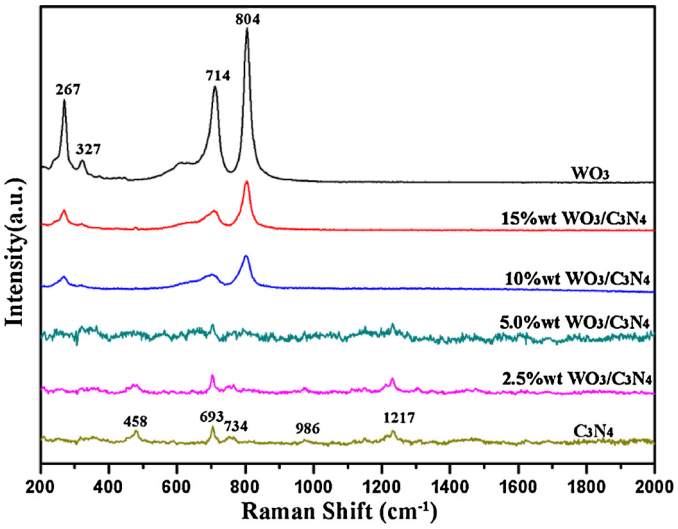

Fig. 4. Raman spectra of g-C_3N_4 with different WO_3 loadings.

Compared the TEM image of 10 wt.% WO_3/g-C_3N_4 to the 5 wt.% one (see Fig. 3d,f), it clearly reveals that vast WO_3 nanorods come to aggregate on the surface and the WO_3 particles grow bigger, which is in accord with the results of crystallite size (from 11–18 nm) in Table 1 calculated by using Scherrer equation.

The Raman spectra, as shown in Fig. 4, illustrate additional information for the structures of WO_3, g-C_3N_4 and WO_3/g-C_3N_4

composites. The Raman bands in Fig. 4a are in good agreement with the standard octahedral crystalline WO_3, at *ca.* 804, 714, 327 and 267 cm^{-1} [32]. Meanwhile, it is clear that the Raman bands in Fig. 4b,c are similar to those of pure WO_3, attributed to certain high content of tungsten species resulting in the agglomeration of microcrystalline WO_3 on the surface of g-C_3N_4. In the g-C_3N_4 sample, the weak characteristic peaks of g-C_3N_4 at 458, 693, 734, 986 and 1217 cm^{-1} were observed (see Fig. 4f). The Raman bands in Fig. 4f at approximately 707 and 986 cm^{-1} are indexed to the different types of ring breathing modes of s-triazine in the g-C_3N_4 crystal structure [33]. Interestingly, compared with that of pure g-C_3N_4, with the increasing amount of WO_3 in WO_3/g-C_3N_4 composites, the intensity of peaks at 707 and 986 cm^{-1} gradually decreases. When the amount of WO_3 exceeds 5 wt.%, the characteristic peaks of WO_3 appear, while the characteristic bands of g-C_3N_4 obviously vanish. This phenomenon may be attributed to a synergistic interaction between s-triazine rings in the g-C_3N_4 crystal structure and WO_3 nanorods. In addition, as discussed above in TEM and XRD results, WO_3 nanorods are well dispersed on the surface of g-C_3N_4 nanosheets.

Surface elements and chemical states of 5% WO_3/g-C_3N_4 nanocomposite are further investigated by XPS method. The C1s spectrum in Fig. 5b reveals two peaks with binding energies of 284.6 and 287.8 eV. The two peaks are respectively ascribed to the sp2-C atoms bonded to three neighboring N atoms and the sp2-hybridized C atoms in the aromatic ring attached to terminal uncondensed amino groups (e.g. —NH_2 and —NH) [34,35]. As shown in Fig. 5c, the N1s spectra can be deconvoluted into three peaks centered at 398.3, 400.3 and 404.0 eV, respectively. The peak at 398.3 eV is assigned to the presence of pyridinic-N species, by which each N atom is bonded to two carbon atoms from the aromatic ring located at the edges of the graphite planes [30]. The peak at 400.3 eV corresponds to N atoms trigonally bonded with sp2- or sp3-C atoms. Whereas, the peak at 404.0 eV is ascribed to the terminal amino groups (-NH_2). These assignments of C1s and N1s agree well with the g-C_3N_4 reported previously [36,37]. However, the surface C/N ratio (2.83) is much higher than 0.75, which may be attributed to part of N-containing species being carbonized at high temperature. Moreover, the W4f spectra in Fig. 5d suggest that both W^{6+} and W^{5+} species at W 4f7/2 (35.2 and 34.2 eV) for the W4f spin-orbit components are identified [38].

3.2. Catalyst activity of the WO_3/g-C_3N_4 composites

For the first time, the novel WO_3/g-C_3N_4 nanocomposites were used as heterogeneous catalyst for the oxidative cleavage of cyclohexene oxide to adipaldehyde by using eco-friendly H_2O_2 as the oxidant and TBP as the solvent. All products of the reaction are determined by GC-MS (see Scheme S1). As shown in Table 2 and Fig. S3, the catalysts are highly active and afford remarkably high (98%) conversion towards the formation of adipaldehyde in very short reaction time (1 h). Moreover, adipaldehyde yield is strongly dependent on the content of WO_3 in the WO_3/g-C_3N_4 composites. It should be noted that 5% WO_3/g-C_3N_4 is the optimum catalyst for this reaction with 98% cyclohexene oxide conversion and 75% adipaldehyde yield. When WO_3 content exceeds 5%, the inevitable agglomeration of WO_3 occurs and the amount of active sites decreased, together with the drop of cyclohexene oxide conversion. Conversely, if the WO_3 content is less than 5%, a low adipaldehyde yield is also obtained. This may be attributed to the decreased amount of active WO_3 species because of the coverage by g-C_3N_4 nanosheets. It is interesting to find that, as shown in Table 2 and Fig. S4, the catalytic performance of WO_3 nanorods with g-C_3N_4 nanosheets as the support is much better than that of the catalyst with the same content of WO_3 on commercial graphite carbon (GC) for the catalytic oxidation, not only in the conversion of cyclohexene oxide (98–30%), but in the yield of adipaldehyde (75–21%). Although the catalytic activity of tungstic acid is commensurate with that of 5 wt.% WO_3/g-C_3N_4, tungstic acid is a homogeneous catalyst and it is very difficult to separate it from the reaction mixture and then reused. Meanwhile, 5 wt.% WO_3/g-C_3N_4 composite prepared by a previously reported physical mixing method, commercial WO_3 and pristine g-C_3N_4 are all employed as catalysts under the identical reaction conditions [15]. However, 5 wt.% WO_3 + g-C_3N_4 and commercial WO_3 both exhibit very low conversion of cyclohexene oxide and pristine g-C_3N_4 was inactive in this reaction.

Table 2
Catalytic performance of cyclohexene oxide oxidation over different catalysts[a]

Catalyst	WO_3 loading (wt. %)	Conversion (%)	Adipaldehyde yield (%)
WO_3/g-C_3N_4	2.5	60	39
WO_3/g-C_3N_4	5.0	98	75
WO_3/g-C_3N_4	10	85	60
WO_3/g-C_3N_4	15	64	47
WO_3	100	7	5
g-C_3N_4	–	–	–
None	–	–	–
WO_3 + g-C_3N_4[b]	5.0	Trace	Trace
WO_3/GC[c]	5.0	30	21
$WO_3 \cdot H_2O$	–	97	63

[a] Reaction conditions: reaction temperature, 35 °C; cyclohexene oxide, 1.00 ml; 86 wt.% H_2O_2 aqueous solution, 0.43 ml; TBP, 7.5 ml; the molar ratio of WO_3:cyclohexene oxide, 2.5:100; reaction time, 1 h.
[b] g-C_3N_4/WO_3 was fabricated by a physical mixing method.
[c] GC refers to the commercial graphite carbon.

It is well-known that glutaraldehyde has been broadly applied in the industry of disinfection, sterilization, the tanning process of leather, environmental protection, water treatment, and oil field [39]. The novel heterogeneous process for the oxidation of cyclohexene oxide can be successfully extended to the oxidation of cyclopentene oxide (see Table S1). 99% conversion and 92% yield towards glutaraldehyde can be obtained, suggesting that the 5 wt.% WO_3/g-C_3N_4 composite is a very promising candidate for its potential application in industry.

3.3. Stability of the WO_3/g-C_3N_4 composites

To further test the practical reusability of the WO_3/g-C_3N_4 catalyst in the oxidative cleavage of cyclohexene oxide to adipaldehyde, a series of recycling tests have been carried out by repeated reaction cycles under the same reaction condition as described above. After each cycle, the catalyst was recovered by simple filtration, washed with water and ethanol three times, then dried at 100 °C for 12 h and reused in the next run. As shown in Fig. 6 and Table S2, the 5 wt.% WO_3/g-C_3N_4 catalyst can be recycled for seven times. No distinct decrease in the catalytic activity and selectivity of 5 wt.% WO_3/g-C_3N_4 in the five cycles could be observed. Notably, there is no distinction between the XRD results before and after the reaction (see Fig. S5), suggesting its structural stability during the oxidation with H_2O_2. This finding differs abruptly with those WO_3-based heterogeneous materials reported earlier (WO_3/SiO_2 [40,41] and WO_3/TiO_2 [42]), the WO_3 species of which aggregated obviously during the recycling test. However, the conversion of cyclohexene oxide gradually drops from 98 to 88% after the fifth cycle and the selectivity to adipaldehyde remains constant. This result implies that the active species are covered by high boiling organic solvent (TBP) and some of the WO_3/g-C_3N_4 catalyst is lost during the course of centrifugation and separation after five cycles' reaction [11]. In addition, leaching of tungsten oxide and homogeneous catalysis of tungsten oxide were excluded by ICP analysis for the filtrate and

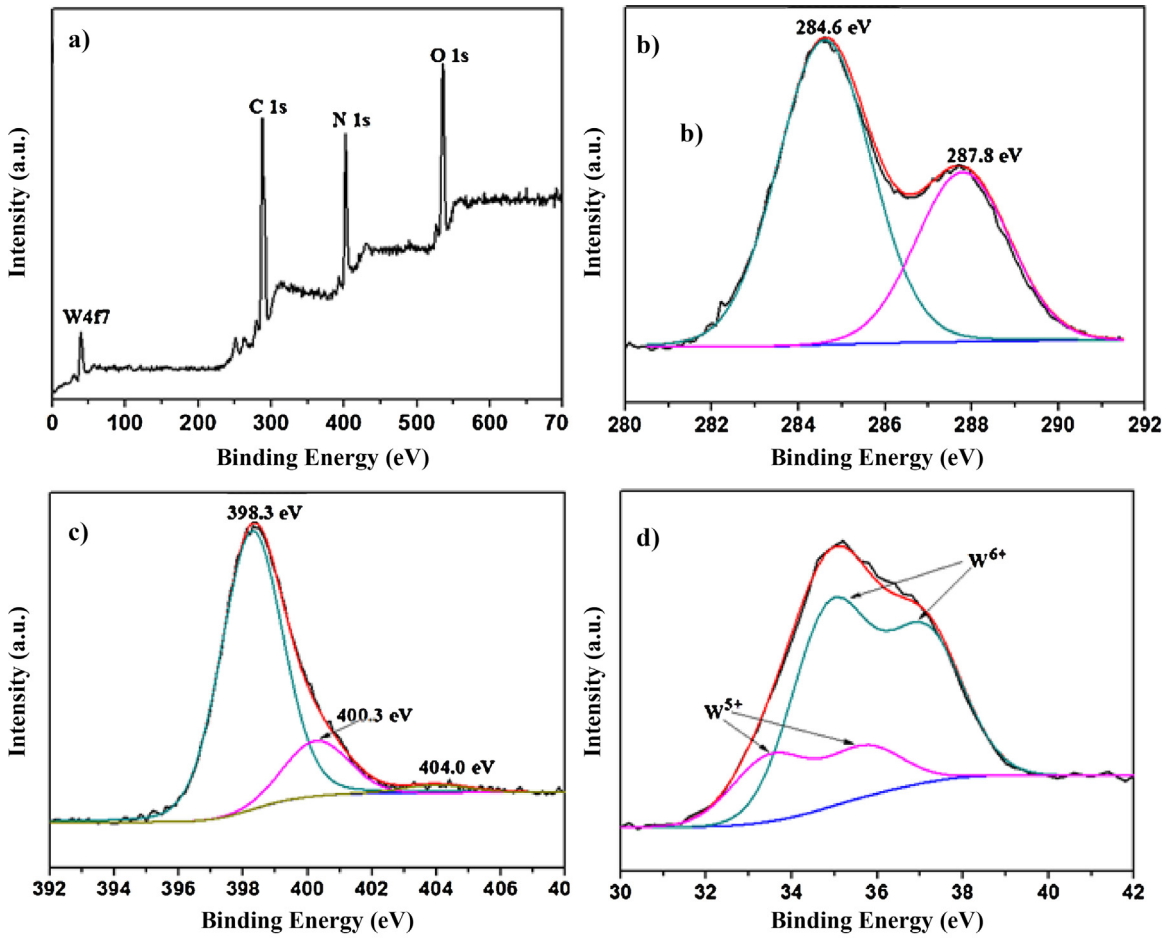

Fig. 5. XPS spectra of 5% WO_3/g-C_3N_4: (a) the survey spectrum; (b) high-resolution C1s; (c) high-resolution N1s; (d) high-resolution W4f.

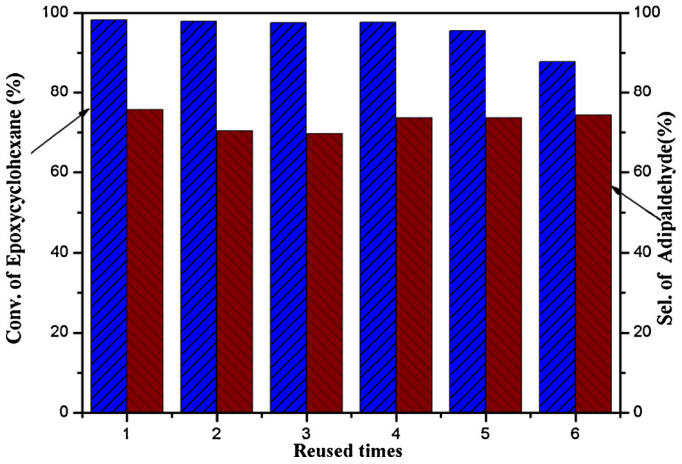

Fig. 6. Recycling of 5 wt.% WO_3/g-C_3N_4 catalyst for the production of adipaldehyde.

the hot-filtration test of the reaction by using the standard method reported elsewhere.

3.4. Possible catalytic oxidation mechanism

Based on the analysis above, a possible catalytic oxidation mechanism of the WO_3/g-C_3N_4 nanocomposites for the oxidative cleavage of cyclohexene oxide to adipaldehyde was proposed and illustrated in Fig. 7. WO_3 nanorods were well dispersed on the surface of g-C_3N_4 nanosheets to get more possible reaction sites of tungsten oxide species. H_2O_2 is activated by the supported WO_3 nanorods to generate the reaction oxygen species [43]. Meanwhile, the nitrogen-neighboring carbon of g-C_3N_4 owns a metal-like *d*-band electronic structure and makes the adjacent carbon more capable to host the formation of reaction oxygen species [44]. Subsequently, cyclohexene oxides interact with the —NH and —NH_2 groups on the surface of g-C_3N_4 sheets through the hydroxyl groups to form strong O···NH interactions and easy access to active sites (tungsten oxide species) and reaction oxygen species on the surface of g-C_3N_4 nanosheets. Through this process, cyclohexene oxide is selectively oxidized to adipaldehyde.

To verify the above assumption of the oxidative cleavage of cyclohexene oxide to adipaldehyde with the help of WO_3/g-C_3N_4 composites as catalysts, several additional experiments were carried out. When small amount of NaF aqueous solution (0.1 mol/l), a scavenger for hydrogen bond of amino groups, was added to the reaction mixture, the conversion of cyclohexene oxide remarkably decreased from 98 to 36% in 1 h (see Fig. S6), suggesting that F^- ions are more easy to access to the —NH or —NH_2 groups on the surface of g-C_3N_4 nanosheets to form more strong F···NH interactions than that of O^{2-} ions to form the O···NH interactions [45]. Hence, cyclohexene oxides can hardly interact with the —NH and —NH_2 groups on the surface of g-C_3N_4 sheets through the hydroxyl groups to form strong O···NH interactions. As a result, the catalytic activity dropped and the conversion of cyclohexene oxides significantly decreased. This finding indicates that the O···NH interactions between cyclohexene oxide and the —NH or —NH_2 groups

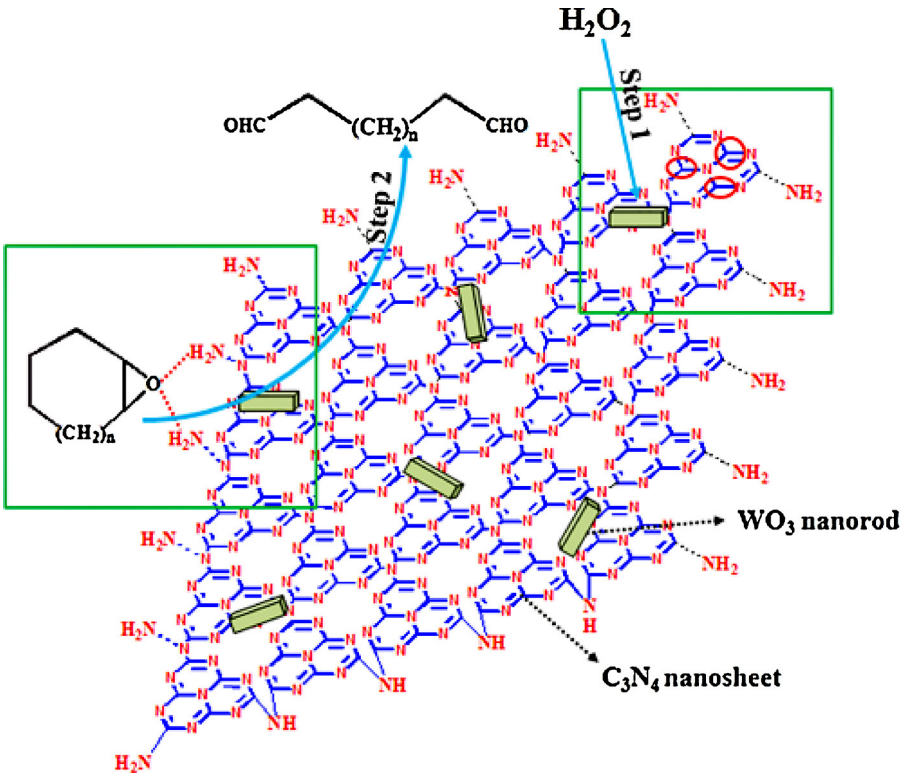

Fig. 7. Possible reaction mechanism of cycloalkene oxides over WO_3/g-C_3N_4 composites.

on the surface of g-C_3N_4 nanosheets play an important role in the oxidative cleavage of cyclohexene oxide. In the present work, the C_3N_4 nanosheets are considered as the support and co-catalyst as well. As the catalyst support, the WO_3 nanorods can be well supported on the surface of g-C_3N_4 nanosheets in an appropriate proportion to get more active sites of tungsten species, which can be clearly seen in the TEM images. Meanwhile, as the co-catalysts, the nitrogen-neighboring carbon of g-C_3N_4 owns a metal-like *d*-band electronic structure and makes the adjacent carbon more capable to host the formation of reaction oxygen species.

In order to illustrate the importance of a metal-like *d*-band electronic structure of the nitrogen-neighboring carbon of g-C_3N_4, 5 wt.% WO_3/graphite carbon without C—N or C=N groups was applied in the present catalytic oxidation reaction. The conversion of cyclohexene oxide obviously dropped from 98 to 30%, as compared with 5 wt.% WO_3/g-C_3N_4. Hence, it is also vital for the green oxidation reaction that the nitrogen-neighboring carbon of g-C_3N_4 with a metal-like *d*-band electronic structure drove cyclohexene oxide and reaction oxygen species to react more easily. Detailed mechanism at molecular level to disclose the intrinsic nature of the present WO_3/g-C_3N_4 composite in the oxidation reaction with aqueous H_2O_2 is being under way.

4. Conclusion

In summary, we demonstrate here a simple, eco-friendly and large-scale method for the ultrasonic-assisted synthesis of nanocomposites with g-C_3N_4 nanosheets decorated by WO_3 nanorods. The novel WO_3/g-C_3N_4 nanocomposites show much higher surface area, excellent catalytic performance and super stability in the oxidative cleavage of cyclohexene oxide to adipaldehyde. The present study put forward a new and eco-friendly method for ultrasonic-assisted synthesis of WO_3/g-C_3N_4 nanocomposites, which might open novel vistas for exploring more metal oxide/g-C_3N_4 nanocomposites for green catalytic oxidation applications.

Acknowledgments

We would like to thank financial support by the Major State Basic Research Development Program (Grant No. 2012CB224804), National Nature Science Foundation of China (Project 21373054, 21173052), State Key Laboratory of Catalytic Materials and Reaction Engineering (RIPP, SINOPEC) and the Natural Science Foundation of Shanghai Science and Technology Committee (08DZ2270500).

Appendix A. Supplementary data

Supplementary data associated with this article can be found, in the online version, at http://dx.doi.org/10.1016/j.apcatb.2014.10.037.

References

[1] N. Ryoji, M. Aoki, K. Sato, Chem. Commun. 16 (2003) 1977.
[2] R. Kumar, S. Sithambaram, S.L. Suib, J. Catal. 262 (2009) 304.
[3] L. Liu, Y. Li, H. Wei, M. Dong, J. Wang, A.M.Z. Slawin, J.P. Li, J.X. Dong, R.E. Morris, Angew. Chem. Int. Ed. 48 (2009) 2206.
[4] H.J. Yan, X.J. Zhang, S.Q. Zhou, X.H. Xie, Y.L. Luo, Y.H. Yu, J. Alloy. Compd. 509 (2011) 232.
[5] Y. Wang, J. Yao, H.R. Li, D.S. Su, M. Antonietti, J. Am. Chem. Soc. 133 (2011) 2362.
[6] Y. Wang, J.S. Zhang, X.C. Wang, M. Antonietti, H.R. Li, Angew. Chem. Int. Ed. 49 (2010) 3356.
[7] P.F. Zhang, Y.T. Gong, H.R. Li, Z.R. Chen, Y. Wang, RSC Adv. 3 (2013) 5121.
[8] P.F. Zhang, H.R. Li, Y. Wang, Chem. Commun. 50 (2014) 6312.
[9] M. Gopa, C.B. Gobinda, S.K. Singh, K.M. Parida, Dalton Trans. 41 (2012) 14299.
[10] J. Engweiler, J. Harf, A. Baiker, J. Catal. 159 (1996) 259.
[11] X.L. Yang, W.L. Dai, C.W. Guo, H. Chen, Y. Cao, H.X. Li, J. Catal. 234 (2005) 438.
[12] R.H. Jin, X. Xia, W.L. Dai, H.X. Li, J.F. Deng, Catal. Lett. 62 (1999) 201.
[13] X.L. Yang, W.L. Dai, R.H. Gao, H. Chen, H.X. Li, Y. Cao, K.N. Fan, J. Mol. Catal. A: Chem. 241 (2005) 205.

[14] X.L. Yang, W.L. Dai, H. Chen, Y. Cao, H.X. Li, H.Y. He, K.N. Fan, Appl. Catal. A: Gen. 283 (2005) 1.
[15] K. Katsumata, R. Motoyoshi, N. Matsushita, K. Okada, J. Hazard. Mater. 260 (2013) 475.
[16] S.F. Chen, Y.F. Hu, S.G. Meng, X.L. Fu, Appl. Catal. B: Environ. 150 (2014) 564.
[17] A. Thomas, A. Fischer, F. Goettmann, M. Antonietti, J.O. Muller, R. Schogl, S. Robert, J.M. Carlsson, J. Mater. Chem. 18 (2008) 4893.
[18] F. Dong, L.W. Wu, Y.J. Sun, M. Fu, Z.B. Wu, S.C. Lee, J. Mater. Chem. 21 (2011) 15171.
[19] J.H. Liu, Y.W. Zhang, L.H. Lu, G. Wu, W. Chen, Chem. Commun. 48 (2012) 8826.
[20] S.C. Yan, Z.S. Li, Z.G. Zou, Langmuir 25 (2009) 10397.
[21] L.Q. Ye, J.Y. Liu, Z. Jiang, T.Y. Peng, L. Zan, Appl. Catal. B: Environ. 142 (2013) 1.
[22] V.N. Khabashesku, J.L. Zimmerman, J.L. Margrave, Chem. Mater. 12 (2000) 3264.
[23] X.F. Li, J. Zhang, L.H. Shen, Y.M. Ma, W.W. Lei, Q.L. Cui, Appl. Phys. A 94 (2009) 387.
[24] S. Katharina, B.M. Maria, D. Viola, Z. Christian, S. Jürgen, V.L. Bettina, J. Am. Chem. Soc. 136 (2014) 1730.
[25] M.J. Bojdys, J.O. Müller, M. Antonietti, A. Thomas, Chem. Eur. J. 14 (2008) 8177.
[26] Z.Y. Zhang, Q.J. Zhu, J. Ding, X. Liu, W.L. Dai, Appl. Catal. A: Gen. 482 (2014) 171.
[27] J. Xu, H.T. Wu, X. Wang, B. Xue, Y.X. Li, Y. Cao, Phys. Chem. Chem. Phys. 15 (2013) 4510.
[28] X.J. Bai, L. Wang, R.L. Zong, Y.F. Zhu, J. Phys. Chem. C 117 (2013) 9952.
[29] Q. Su, J. Sun, J.Q. Wang, Z.F. Yang, W.G. Cheng, S.J. Zhang, Catal. Sci. Technol. 4 (2014) 1556.
[30] A.B. Chen, Y.F. Yu, H.J. Lv, Y.Y. Wang, S.F. Shen, Y.Q. Hu, B. Li, Y. Zhang, J. Zhang, J. Mater. Chem. A 1 (2013) 1045.
[31] X.J. Bai, R.L. Zong, C.X. Li, D. Liu, Y.F. Liu, Y.F. Zhu, Appl. Catal. B: Environ. 147 (2014) 82.
[32] J.G. Graselli, B.J. Bullkin, Analytical Raman Spectroscopy, John Wiley, New York, 1991, pp. 352.
[33] P.V. Zinin, L.C. Ming, S.K. Sharma, V.N. Khabashesku, X.R. Liu, S.M. Hong, Chem. Phys. Lett. 472 (2009) 69.
[34] Y.L. Gu, L.Y. Chen, L. Shi, J.H. Ma, Z.H. Yang, Y.T. Qian, Carbon 13 (2003) 2674.
[35] S.N. Talapaneni, S. Anandan, G.P. Mane, C. Anand, D.S. Dhawale, S. Varghese, J. Mater. Chem. 22 (2012) 9831.
[36] S.S. Park, S.W. Chu, C. Xue, D. Zhao, C.S. Ha, J. Mater. Chem. 21 (2011) 10801.
[37] E.R. Pinero, D.C. Amorós, A.L. Solano, J. Find, U. Wild, I.R. Schlog, Carbon 40 (2002) 597.
[38] M. Valigi, D. Gazzoli, I. Pettiti, G. Mattei, S. Colonna, S.D. Rossi, G. Ferraris, Appl. Catal. A: Gen. 231 (2002) 159.
[39] Q.J. Zhu, X.F. Chu, Z.Y. Zhang, W.L. Dai, K.N. Fan, RSC Adv. 3 (2013) 1744.
[40] G. Lu, X.Y. Lia, Z.P. Qua, Y.X. Wang, G.H. Chen, Appl. Surf. Sci. 255 (2008) 3117.
[41] R.H. Jin, H.X. Li, J.F. Deng, J. Catal. 203 (2001) 75.
[42] G. Lua, X.Y. Li, Z.P. Qu, Q.D. Zhao, H. Li, Y. Shen, G.H. Chen, Chem. Eng. J. 159 (2010) 242.
[43] J.F. Deng, X.H. Xu, H.Y. Chen, A.R. Jiang, Tetrahedron 48 (1992) 3503.
[44] W.J. Li, Y.J. Gao, W.L. Chen, P. Tang, W.Z. Li, Z.J. Shi, D.S. Su, J.G. Wang, D. Ma, ACS Catal. 4 (2014) 1261.
[45] E. Haque, J.W. Jun, S.N. Talapaneni, A. Vinu, S.H. Jhung, J. Mater. Chem. 20 (2010) 10801.